Supporting Information

Flexible Graphene Films via the Filtration of Water-Soluble Noncovalent Functionalized Graphene Sheets

Yuxi Xu, Hua Bai, Gewu Lu, Chun Li, and Gaoquan Shi**

Key Laboratory of Bioorganic Phosphorus Chemistry & Chemical Biology, Department of Chemistry, Tsinghua University, Beijing 100084, People's Republic of China

1. Synthesis of Graphite Oxide (GO)

Graphite oxide (GO) was synthesized from natural graphite powder by a modified Hummers method.[1,2] Graphite powder (3 g, 325 mesh) was put into an 80 °C solution of concentrated H_2SO_4 (12 mL), $K_2S_2O_8$ (2.5 g), and P_2O_5 (2.5 g). The mixture was kept at 80 °C for 4.5 h using a hotplate. Successively, the mixture was cooled to room temperature and diluted with 0.5 L of de-ionized (DI) water and left overnight. Then, the mixture was filtered and washed with de-ionized (DI) water using a 0.2 micron Nylon Millipore filter to remove the residual acid. The product was dried under ambient condition overnight. This pre-oxidized graphite was then subjected to oxidation by Hummers' method described as follows. Pretreated graphite powder was put into cold (0 °C) concentrated H_2SO_4 (120 mL). Then, $KMnO_4$ (15 g) was added gradually under stirring and the temperature of the mixture was kept to be below 20 °C by cooling. Successively, the mixture was stirred at 35 °C for 2 h, and then diluted with DI water (250 mL). Because the addition of water in concentrated sulfuric acid medium released a large amount of heat, the addition of water was carried out in an ice bath to keep the temperature below 50 °C.

After adding all of the 250 mL of DI water, the mixture was stirred for 2 h, and then additional 0.7 L of DI water was added. Shortly after the dilution with 0.7 L of water, 20 mL of 30% H_2O_2 was added to the mixture, and the color of mixture changed into brilliant yellow along with bubbling. The mixture was filtered and washed with 1:10 HCl aqueous solution (1 L) to remove metal ions followed by 1 L of DI water to remove the acid. The resulting solid was dried in air and diluted to make a GO dispersion (0.5% w/w). Finally, it was purified by dialysis for one week to remove the remaining metal species.

Exfoliation was carried out by sonicating 0.1 mg mL^{-1} GO dispersion under ambient condition for 20 min. The resulting homogeneous yellow-brown dispersion was tested to be stable for several months and used for reduction.

2. Instrumentation of Atomic Force Microscopy (AFM) and UV-visible (UV-vis) Spectroscopy.

Atomic force microscopic (AFM) images were taken out using a Nanoscope III MultiMode SPM (Digital Instruments) with an AS-12 ("E") scanner operated in tapping mode in conjunction with a V-shaped tapping tip (Applied Nanostructures SPM model: ACTA). The images were taken at a scan rate of 2 Hz. UV-vis spectra were recorded on a U-3010 spectrometer. Fluorescence spectra were recorded on a Perkin-Elmer LS55 luminescence spectrometer.

3. XRD Patterns of Graphite and GO.

Figure S1 shows XRD patterns of GO and natural graphite that were obtained by using a D8 Advance (Bruker) X-ray diffractometer with Cu K_α radiation (λ = 1.5418 Å). The pattern of GO has a peak centered at $2\theta = 11.4^o$, corresponding to the (002) inter-planar spacing of 7.75 Å. The most intense peak for graphite at $2\theta = 26.4^o$ (corresponding to a *d*-spacing of 3.35 Å) is absent in GO sample.

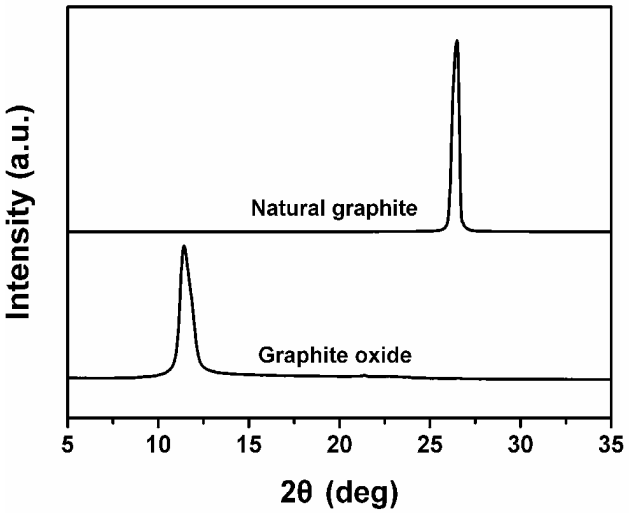

Figure S1. XRD patterns of graphite oxide and natural graphite.

4. FT-IR Spectrum of GO

FT-IR spectrum of GO illustrated in Figure S2 also confirms the successful oxidation of graphite. The characteristic vibrations are the broad and intense peak of O–H groups centered at 3400 cm^{-1}, strong C=O peak at 1740 cm^{-1}, the O–H deformation peak at 1420 cm^{-1}, the C–OH stretching peak at 1220 cm^{-1}, and the C–O stretching peak at 1050 cm^{-1}. The peak at 1620 cm^{-1} was assigned to the vibrations of the adsorbed water molecules and also the contributions from the skeletal vibrations of un-oxidized graphitic domains.

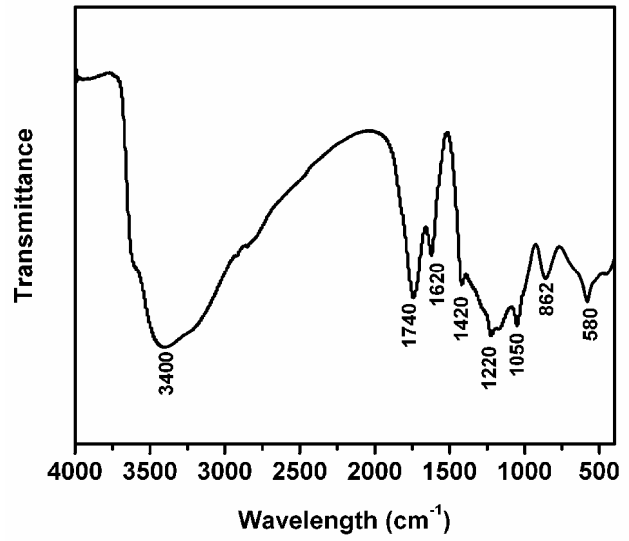

Figure S2. FT-IR spectrum of the as-prepared graphite oxide.

5. Raman Spectra of GO, Reduced GO (r–GO), and PB^--functionalized Graphene (PB^-–G)

Raman spectra were recorded from 1700 to 1100 cm^{-1} on a RM 2000 Microscopic confocal Raman spectrometer (Renishaw PLC, England) using a 633 nm He-Ne laser beam. As shown in Figure S3, the Raman spectrum of GO displays two prominent peaks at 1600 and 1334 cm^{-1}, which correspond to the well-documented G and D bands. The Raman spectrum of r-GO also has both G and D bands (at 1595 and 1330 cm^{-1}, respectively). However, the D/G intensity ratio is increased in comparison with that of the GO spectrum. In the case of PB^-–G, the presence of PB^- resulted in the appearance of a shoulder band around 1612 cm^{-1} and another weak band at 1230 cm^{-1}, and also the distortion of G and D bands (at 1587 and 1330 cm^{-1}, respectively).[3] The Raman spectral results described above agree well with those reported by Stankovich,[4] indicating that the GO has been well deoxygenated in r–GO and PB^-–G.

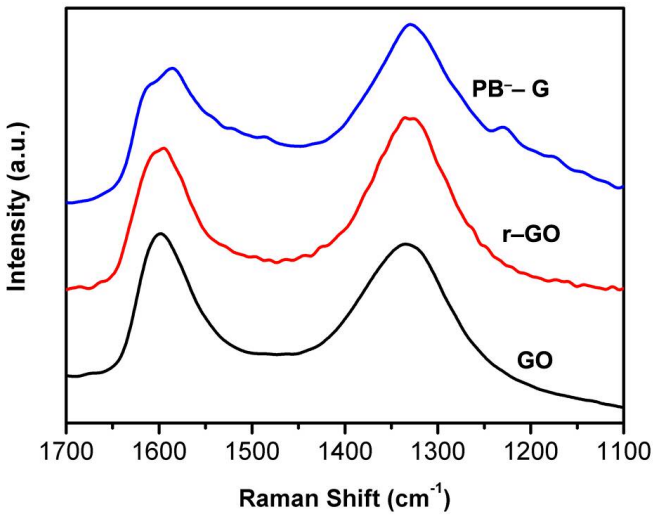

Figure S3. 633 nm exicted Raman spectra of GO, r–GO, and PB^-–G.

6. X-ray Photoelectron Spectroscopic (XPS) Spectra of GO, r–GO, and PB^-–G

XPS measurements were performed on a PHI 550 EACA/SAM photoelectron spectrometer using Al K_α (1486.6 eV) radiation. The C 1s XPS spectrum of GO (Figure S4a) indicates the presence of four types of carbon bonds: C–C (284.5 eV), C–O (286.6 eV), C=O (287.8 eV), and O–C=O (289.0 eV).

Although the C 1s XPS spectra of r–GO (Figure S4b) and PB^{-}–G (Figure S4c) also exhibit the same species, the peak intensities of oxide species are much weaker than those in the spectrum of GO, suggesting considerable de-oxygenation by the reduction process. Besides, there exists an additional component at 285.8 eV, corresponding to the C in the C=N bonds of hydrazone.[5]

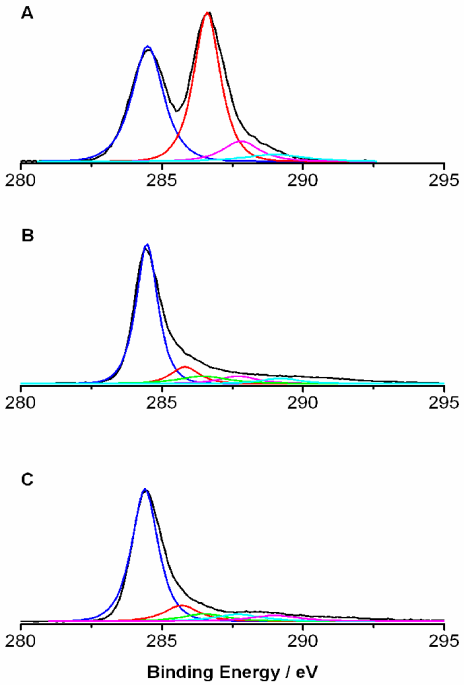

Figure S4. The C 1s spectra of A) GO, B) reduced GO, and C) PB^{-}–G

7. XRD Pattern of PB^{-}–G Film

The characteristic peak (2θ) in the XRD pattern of a PB^{-}–G film (Figure S5) is appeared at 25.4°, corresponding to the layer-to-layer distance (*d*-spacing) of ~0.35 nm. This value is close to the *d*-spacing (0.335 nm) of natural graphite. Another peak at 21.4° may be caused by PB^{-} embedded in PB^{-}–G film, because repeated washing can decrease the intensity of this peak. This result further confirms the well-packed layered structure of the PB^{-}–G film, being consistent with that of the SEM characterization.

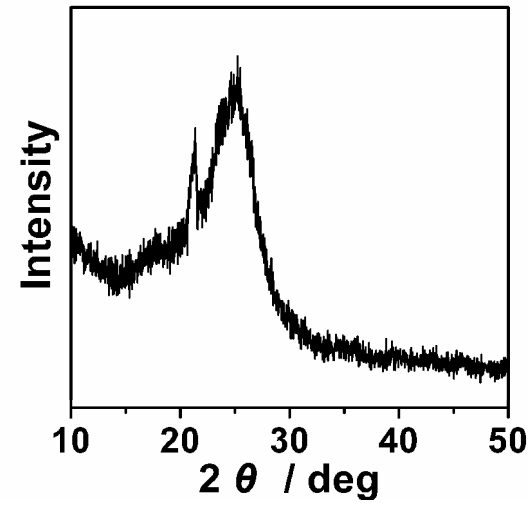

Figure S5. XRD pattern of PB^{-}–G film

8. Mechanical Property of PB^{-}–G Film

Mechanical property tests were conducted with an electronic stretching machine (WDW 3020 Autograph, Changchun Xinke Co., China). The samples were gripped using film tension clamps with a clamp compliance of about 0.2 μm/N. All tensile tests were performed in controlled force mode with a preload of 0.001 N and at a strain ramp rate of 0.05 mm/min. Tensile modulus is determined by fitting the stress-strain plot in the "elastic" regime with a straight line.

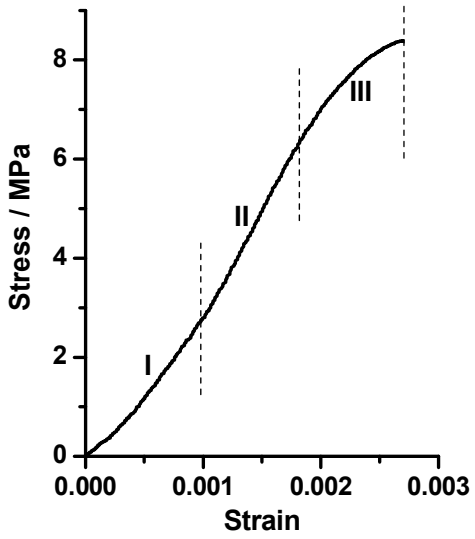

Figure S6. Stress-strain curve for a 30 μm-thick PB^{-}–G film. The deformation can be divided into three regimes: (I) straightening, (II) 'elastic' and (III) plastic.

It can be seen from Figure S6, that the tensile strength and modulus in "elastic" regime of the film were measured to be about 8.4 MPa and 4.2 GPa, respectively. Compared with the strong graphite oxide paper, the graphene film shows nearly a magnitude lower mechanical strength. As stated in ref. 6, the astonishing mechanical properties of graphite oxide paper were derived from the unique interlocking-tile arrangement of the nanoscale graphene oxide sheets through the strong interactions of carboxyl and hydroxyl groups.[6] For the graphene-based film prepared by us, two possible reasons are responsible for its lower mechanical properties. On the one hand, there are few of oxygen functional groups remained in graphene sheets after reduction of graphite oxide and the flexible graphene-based film consists of pyrenebutyrate-functional graphene (PB^-–G) sheets through π-stacking interactions which is prone to slide during stretching the film. Therefore, the friction between basal planes of graphene sheets will be significantly weaker than that of graphite oxide sheets. This may explains why the pyrenebutyrate-functional graphene film possesses similar mechanical performance with flexible graphite foils composed of stacked platelets of expanded graphite.[7] On the other hand, the graphene film in the present work is obtained from filtration of a dispersion of PB^-–G sheets and unavoidably there are some attached and even trapped pyrenebutyrate (PB^-) molecules remained in the resulting film. Therefore, in this sense, the graphene film examined here is a composite film, and the existence of small molecules would further decrease the mechanical properties. Although the graphene-based film has lower mechanical property than graphite oxide paper, the film with high conductivity will still be attractive for practical applications.

9. Application of PB^-–G in Dye Sensitized Solar Cell (DSSC)

PB^-–G was spin-coated on a fluorine-doped tin oxide (FTO) substrate using its 0.1 mg/mL dispersion at a spin rate of 450 rpm. The graphene-modified FTO (G/FTO) was used as the counter electrode in DSSC. For control experiments, bare FTO or platinum-coated FTO (Pt/FTO) was used as

the counter electrode. All control experiments were performed under the same conditions. The nanocrystalline TiO_2 photoelectrode, FTO and platinum-coated FTO were purchased from Heptachroma Solar Tech. A ruthenium dye, cis-bis(isothiocyanato)bis(2,2'-bipyridyl-4-carboxilic acid-4'-tetrabutylammonium carboxylate)ruthenium(II) (N719 dye: purchased from Solaronix) was used as a sensitizer for the TiO_2 particles. The electrolyte consisted of 0.12 mol/L iodine, 0.10 mol/L lithium iodide, 1.0 mol/L 1,2-dimethyl-3-propylimidazolium iodide, and 0.50 mol/L 4-tert-butylpyridine in 3-methoxyacetonitrile. The conversion efficiencies were measured under simulated sun light (AM 1.5, 100 mW/cm^2). The area of the TiO_2 photoelectrode was 0.23 cm^2.

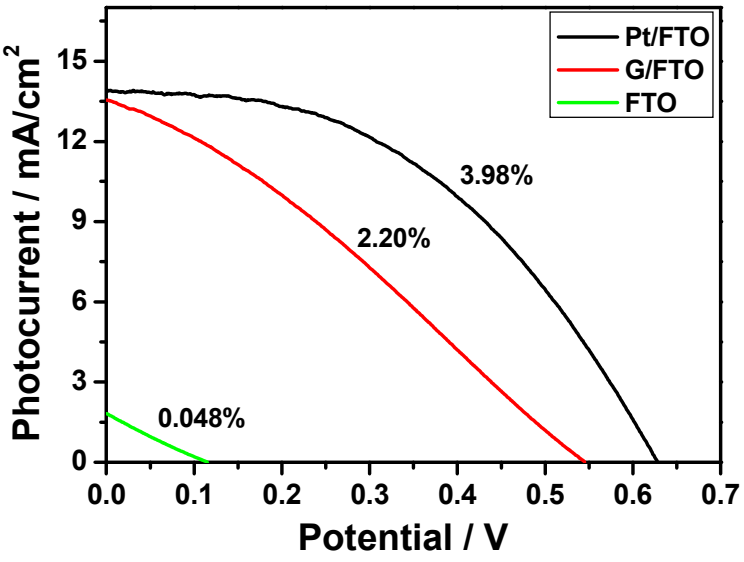

Figure S7. Photocurrent density-voltage curves of the DSSCs under 1.5 AM, 100 mW/cm^2 illumination.

As shown in Figure S7, G/FTO DSSC shows greatly improved performance compared with that of the bare FTO DSSC but still poorer than that of the Pt/FTO DSSC. The energy conversion efficiency of the FTO DSSC was calculated to be 0.048%, and it was increased to 2.2 % for a G/FTO DSSC. The short-circuit currents of G/FTO and Pt/FTO DSSCs were close, while the fill factor and open-circuit potential of G/FTO DSSC were slightly lower. We believe that the performance of G/FTO DSSC can be further improved through optimizing the constructions of the device. These results indicate that the

soluble graphene sheets can be used as a promising electrocatalytic material and have potential applications in DSSCs.

Supplementary References.

(1) Kovtyukhova, N. I.; Ollivier, P. J.; Martin, B. R.; Mallouk, T. E.; Chizhik, S. A.; Buzaneva, E. V.; Gorchinskiy, A. D. *Chem. Mater.***1999**, *11*, 771.

(2) Hummers, W. S.; Offeman, R. E. *J. Am. Chem. Soc.* **1958**, *80*, 1339.

(3) Lu, G. W.; Shi, G. Q. *J. Electroanal. Chem.* **2006**, 586, 154.

(4) Stankovich, S.; Dikin, D. A.; Piner, R. D.; Kohlhaas, K. A.; Kleinhammes, A.; Jia, Y.; Wu, Y.; Nguyen, S. T.; Ruoff, R. S. *Carbon* **2007**, *45*, 1558.

(5) Stankovich, S.; Piner, R. D.; Chen, X. Q.; Wu, N. Q.; Nguyen, S. T.; Ruoff, R. S. *J. Mater. Chem.* **2006**, *16*, 155.

(6) Dikin, D. A.; Stankovich, S.; Zimmy, E. J.; Piner, R. D.; Dommett, G. H. B.; Evmenenko, G.; Nguyen, S. T.; Ruoff, R. S. *Nature* **2007**, *448*, 457.

(7) Leng, Y.; Gu, J.; Cao, W.; Zhang, T. Y. *Carbon* **1998**, *36*, 875.